Determination of guided-mode resonances in photonic crystal slabs

Pierre Pottier, Lina Shi, and Yves-Alain Peter*

Department of Engineering Physics, Ecole Polytechnique de Montréal, Montréal, Quebec H3C 3A7, Canada
**Corresponding author: yves-alain.peter@polymtl.ca*

Received September 9, 2011; revised October 9, 2011; accepted October 9, 2011;
posted October 14, 2011 (Doc. ID 154072); published December 9, 2011

We present a design and analysis study of guided-mode resonances in photonic crystal slabs. Three-dimensional finite-difference time-domain (FDTD) simulations are used in parallel with a simplified model of guided-mode resonances to produce a representation of their evolution with structural parameters. From the analysis of the effective medium behavior of the system, we propose a simplified method able to predict the first guided-mode resonances at normal incidence with a good accuracy (~1%) for holes with radius-to-period ratio smaller than 0.3 for the transverse magnetic polarization created internally. A substantial gain of time is, therefore, provided compared to FDTD (from the hours level to the seconds level). We also focus on two other important parameters, the quality factor and asymmetry of peaks, and present a way to design symmetric peaks with low sidebands.

OCIS codes: 230.5298, 260.5740, 310.6805, 230.7408, 230.4040, 050.2065.

1. INTRODUCTION

Guided-mode resonances [1–3] result from the interaction of waves propagating in free space with waves guided in a waveguide. Such an interaction is made possible by periodic structure in the waveguide, turning it into a leaky waveguide and allowing coupling of leaky-guided and radiated modes. This results, in terms of the transmission spectrum, in Fano-shaped peaks overlapping the background transmission across the waveguide layer. The guided-mode resonances are angle and polarization dependent [4].

Devices using guided-mode resonances present interest for several kinds of applications. Guided-mode resonances can show arbitrarily narrow peaks, which can be used to make optical filters with very high quality factors [5,6]. On the other hand, high-reflection mirrors with wide bands can also be created [7]. Various functions in the optical transmission can thus be designed; in particular, large group delay can be obtained [8,9]. These features can be achieved in a single layer, in comparison to multilayer Bragg filters, which can need a hundred layers. Structures supporting guided-mode resonances, such as photonic crystals (PhCs), are, therefore, very appropriate for integration in a compact device. In addition, the high electromagnetic fields that can be obtained in the guided-mode resonator can be used to enhance the signal obtained from fluorescent elements, making possible high-sensitivity biosensors [10–12]. One or several membranes supporting guided-mode resonances can be inserted in microelectromechanical systems (MEMS), enabling tunability of the optical response [12–14]. Such configuration can also be used as a displacement sensor [15].

The guided-mode resonance phenomenon has been described in the literature, and analytical expressions have been derived to reproduce the shape of the transmission spectrum [16]. But no analytic expression is available for the position of guided-mode resonances.

Here, we use a Si_3N_4 system—a membrane surrounded by air—that exhibits advantages such as transparency in the visible range and a significant refractive index (taken here fixed as $n_2 = 2.05$). We use two-dimensional (2D) PhCs [17] for an effect in all directions of the plane, and with a square lattice, which makes it independent of polarization, at normal incidence.

A first question we want to answer is which parameters, among thickness (t), period (a), and radius (r), of the PhC slab should be used to get a guided-mode resonance at a given wavelength. We first discuss the limit case, when the hole radii tend to zero. Then we perform simulations for the general case (various radii), using the FDTD algorithm. We represent the answer to the question in a multiple graph, linking the parameters together. We also extract and represent two result parameters, the quality factor and asymmetry of reflection peaks, which are important elements entering into the design of a structure. We show that symmetric peaks with very low sideband reflection can be designed using antireflection coating. Furthermore, we try to dissociate the general problem of guided-mode resonances into the positions of the resonances and the background reflection. We extract the effective index of the structure, when seen as a homogeneous medium for transmission across, and compare it with theory. We then, finally, come back to the comparison between infinitely small holes and the general case by reallocating an effective index in the simplified model.

2. INFINITELY SMALL HOLES

Let us first consider a membrane of index n_2, surrounded by a medium of index n_1 (air here, $n_1 = 1$), and perforated by infinitely small periodic holes (period a). Because we neglect the size of the holes, the effective index of the planar waveguide, n_{eff}, is not modified, but the periodicity introduces the folding of the waveguide dispersion curves into the first Brillouin zone. Therefore, the point at angular frequency ω_1

corresponding to in-plane wave vector $k_x = 2\pi/a$ folds back to $k_x = 0$ (normal incidence). Since $\omega/k = c/n_{\text{eff}}$, we get $\omega_1 = 2\pi c/(n_{\text{eff}} \cdot a)$, or

$$\frac{a}{\lambda_1} = \frac{1}{n_{\text{eff}}}. \tag{1}$$

This is the normalized frequency (period over wavelength) at which the first guided-mode resonance for normal incidence will occur.

We will now represent the position of the frequency of the guided-mode resonance in relation to the physical parameters t and a. To keep the case general and dimensionless, we will plot the normalized frequency (a/λ) versus the normalized thickness. There are two possible ways to define the normalized thickness: t/λ and t/a. Both will be represented. The effective index of a planar waveguide, with the aforementioned parameters, is the solution of the equation $f(x) = 0$ [18], with

$$f(x) = 2\pi \frac{t}{\lambda}\sqrt{n_2^2 - x^2} - 2\arctan\left(\eta_{21}\sqrt{\frac{x^2 - n_1^2}{n_2^2 - x^2}}\right) - m\pi, \tag{2}$$

with $\eta_{21} = 1$ for TE polarization and $\eta_{21} = (n_2/n_1)^2$ for TM polarization, and with m the order of the mode. The term "transverse" (electric or magnetic) relates to the plane of incidence of a wave propagating through the interface between the membrane and the surrounding material. We will study the case of the fundamental mode ($m = 0$). For each value of normalized thickness t/λ, we calculate numerically the effective index, which, in turn, gives us the normalized frequency a/λ. Figure 1 shows a/λ versus t/λ for TE and TM polarizations. We also produce it versus t/a by using the relation $t/a = (t/\lambda)/(a/\lambda)$. Since the effective index of a waveguide is contained between the core and cladding indices ($n_1 < n_{\text{eff}} < n_2$), we have, for lower and upper limits of the guided-mode resonance, normalized frequencies:

$$\frac{1}{n_2} < \frac{a}{\lambda} < \frac{1}{n_1}. \tag{3}$$

The lower limit corresponds to an infinitely thick waveguide; therefore, the curve a/λ versus t/λ (or t/a) tends to that lower limit when t/λ (or t/a) tends to infinity. The upper limit corresponds to an infinitely thin waveguide; therefore, the curve a/λ versus t/λ (or t/a) tends to that upper limit when t/λ (or t/a) tends to zero. The upper limit also corresponds (for a finite nonzero thickness) to the case where the size of the material between the holes tends to zero, i.e., when the normalized radius r/a tends to $\sqrt{2}/2$ for the case of a 2D square lattice of circular holes—the index of the "membrane" then becoming n_1. Therefore, we expect, when the hole size will vary, the guided-mode resonance normalized frequencies to lie between the upper limit $1/n_1$ and the curve a/λ versus t/λ represented here (for infinitely small holes).

The planar waveguide allows only one mode (the fundamental) to propagate when [19]

$$\frac{t}{\lambda} < \frac{1}{2\sqrt{n_2^2 - n_1^2}}, \tag{4}$$

i.e., when $t/\lambda \lesssim 0.279$ in our case. Above this value, the first-order mode is also allowed, and will generate an additional guided-mode resonance. In terms of t/a, since Eq. (3) is still true, this happens above ~0.279. The frequency of this higher-order mode is also higher. As a result, the additional curve a/λ versus t/λ or t/a will be of similar shape, just shifted to higher normalized thickness, starting from the critical value calculated, and shifted to higher normalized frequency.

Also, a second guided-mode resonance will appear, corresponding to the second folding of the dispersion curves, i.e., for the normalized frequency

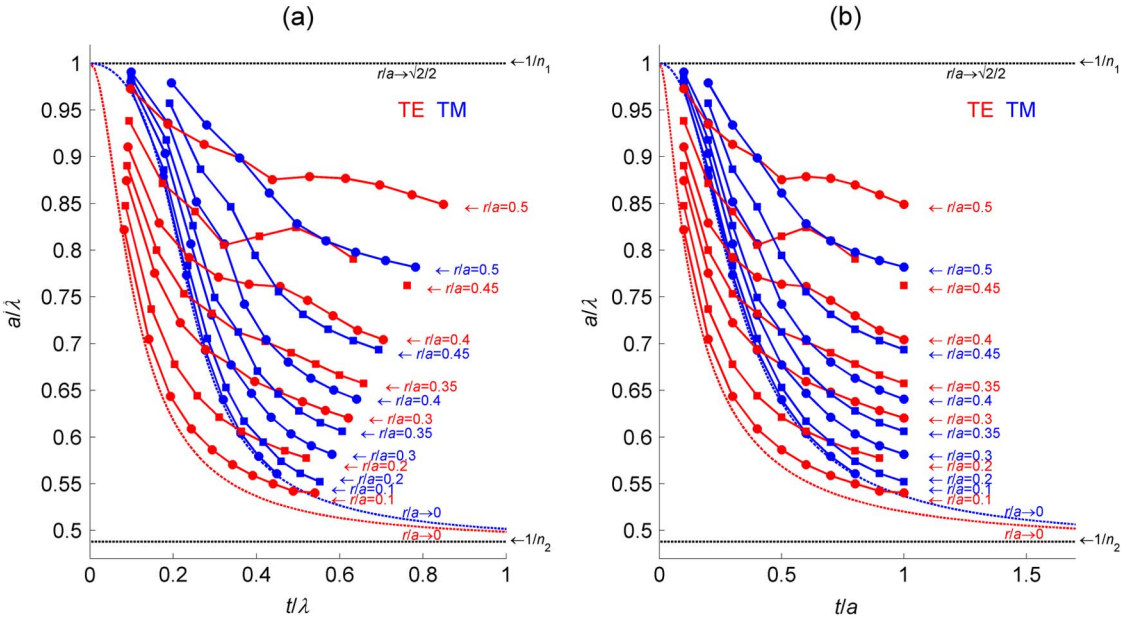

Fig. 1. (Color online) Positions of guided-mode resonances in normalized frequency a/λ versus the normalized thickness of the PhC membrane (a) t/λ or (b) t/a. The color dotted lines are for the limit case of infinitely small holes. The color solid lines correspond to 3D FDTD simulations for several hole normalized radii r/a. Red denotes TE polarization and blue is TM for the light inside the membrane, as defined in the main text.

$$\frac{a}{\lambda_2} = \frac{2}{n_{\text{eff}}}. \tag{5}$$

In our case, this second guided-mode resonance will almost not overlap with the region where the first appears. It would not at all if $n_2 < 2n_1$.

Note also that diffraction of light from the periodic structure in the surrounding medium will appear when

$$\frac{a}{\lambda} > \frac{1}{n_1}. \tag{6}$$

As a consequence, the region where guided-mode resonance will be "isolated", i.e., far from another one and with free side bands, thus good to be exploited as, e.g., a filter with rejected sidebands, is the left and lower region of the diagram in Fig. 1 above the dotted line curve.

3. HOLES OF VARYING RADIUS

We will now discuss the general case with varying hole size. The Section 2 was free from lattice and polarization dependence. We will now focus our study to a 2D square lattice of circular holes (radius r, period a). Considering normal incidence, it is polarization independent. We used the three-dimensional (3D) FDTD algorithm [20] with lateral periodic boundary conditions, and up and down perfectly matched layers. The unit cell is represented in Fig. 2. For each value of normalized thickness t/a, for a given normalized radius r/a, we calculate numerically the reflection (R) spectrum of the structure. We then repeat it for various r/a, and we can dress the maps of evolution of R in normalized frequency a/λ versus normalized thickness t/a, when r/a is varying (Fig. 3). We then extract the position of the peaks (a/λ), and plot it versus t/a, for the various r/a [Fig. 1(b)]. We also use the relation $t/\lambda = (t/a)(a/\lambda)$ to report the data in Fig. 1(a). We can see on Fig. 3 and then more clearly on Fig. 1 that the guided-mode resonances (taken here as the position of maximum of reflection) brush against the curve of infinitely small holes when r/a is small, and then move away as r/a increases, which is what we expected. From Fig. 3, we can observe the first guided-mode resonances (first folding of dispersion curve and mode $m = 0$) on the bottom left part (arrow A gives an example), as well as the next guided-mode resonances (first folding and mode $m = 1$), which is more up and right (arrow B) as we expected from Section 2. We notice that there are

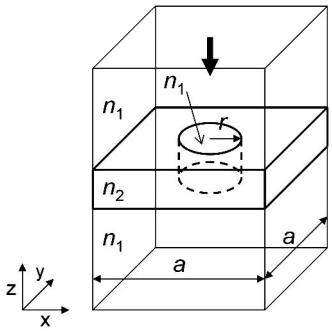

Fig. 2. Unit cell of the PhC membrane used in the FDTD calculations, with period a, radius r, and indices of refraction n_1 and n_2. A plane wave is launched from the top (bold arrow). Reflected and transmitted power is monitored, respectively, at the top and bottom surfaces.

actually two kinds of first guided-mode resonances. In the case of infinitely small holes, we saw there were two possibilities: the two polarizations of the waveguide mode. To confirm this for the case for varying hole size and to identify the modes, we calculated the band diagram of the PhC membrane structure. The band structures are calculated using the previous 3D FDTD algorithm, as detailed in [21]. The results from band diagram calculations (not reported here) agree closely with the FDTD reflection spectra in terms of position of the bands at $k_x = 0$ compared to the position of the reflection peaks. We also identified which are the TE and TM modes; these are reported in Fig. 1. This identification also agrees with the intuitive idea that a curve for a given polarization will be continuous (note that the curves for the two polarizations are crossing), and will undergo a progressive change when r/a increases from 0.

In order to design a guided-mode resonance for a desired wavelength, there are three parameters that need to be chosen (the others are fixed in this study): t, a, and r. But there are two degrees of freedom, as the space of possible guided-mode resonances is the 2D space of Fig. 1, plus the binary choice of the internal polarization. Once a point $(t/\lambda, a/\lambda)$ is chosen in the Fig. 1(a) diagram, t and a get determined, and r is obtained from the r/a value read directly. If additional desired parameters are set, such as the quality factor and/or asymmetry of peak presented in the next two sections, the two degrees of freedom will be further reduced down to one or zero, in this case completely determining the physical dimensions.

4. QUALITY FACTOR

The quality factor (Q) represents the strength of a resonance and is measured as

$$Q = \frac{\nu_r}{\Delta\nu}, \tag{7}$$

with ν_r the frequency of the resonance, and $\Delta\nu$ its FWHM. $\Delta\nu = \nu_2 - \nu_1$, with ν_1 and ν_2 the frequencies at half-maximum, $\nu_2 > \nu_1$. From the FDTD reflection spectra obtained (represented in Fig. 3) we extract the Q value when ν_1 and ν_2 are defined (which is not always the case as the peaks superimpose on the background and are sometimes less than twice tall). For each couple of point $(t/\lambda, a/\lambda)$ or $(t/a, a/\lambda)$, we represent Q in Figs. 4(a) and 4(b). The parameter space is the same as in Fig. 1, and the normalized radius can also be read from the correspondence. Q is represented as a number (superimposed), centered on the data point, and on a color scale, with interpolation between these points. The interpolation is only a guide for the eyes, as it appears even where no value of Q is defined. Figures 4(a) and 4(b) actually correspond to TE internal polarization. The same is represented for TM internal polarization in Figs. 4(c) and 4(d).

In a simplified view of the PhC membrane system, we can say that, at low normalized radius value, the holes will radiate little light, i.e., they represent a low leaking mechanism. Therefore, the residence time in the (leaky) waveguide is high and so is the quality factor of the guided-mode resonance. This is reflected in the graphs close to the limit line of infinitely small holes where high Q or sharps peaks of guided-mode resonance are recorded. Note that all the guided-mode resonances could not be assigned a Q value, but they all show narrow peaks in this region. Also, lower quality factors are

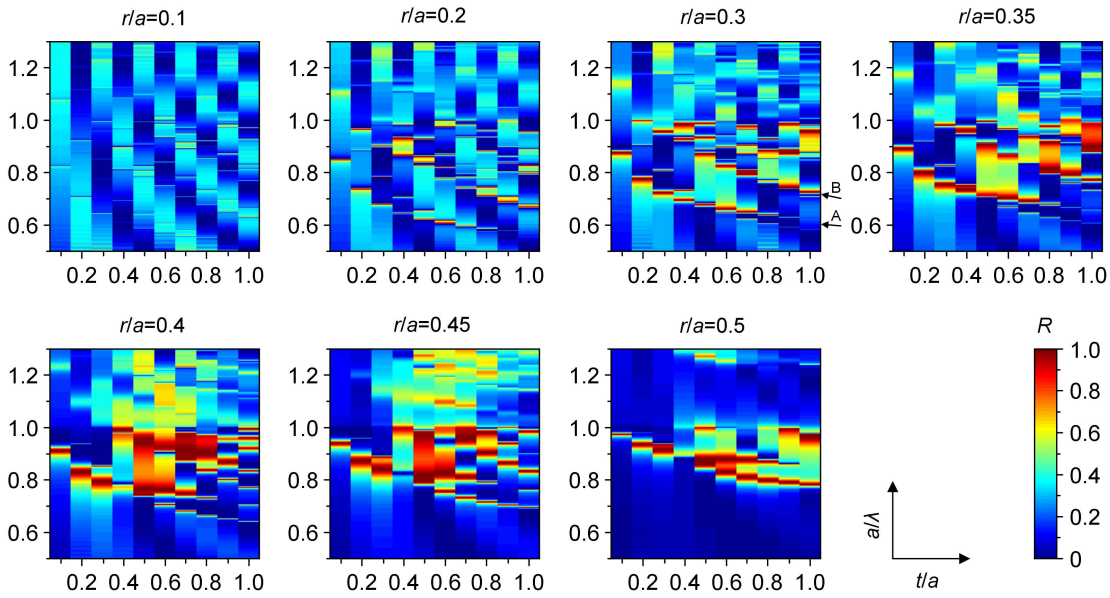

Fig. 3. (Color online) Reflection R (color scale) of the PhC membrane versus normalized frequency a/λ (vertical axis) and normalized thickness t/a (horizontal axis) for varying normalized radius r/a. For $r/a = 0.3$ are exemplified the first guided-mode resonances (arrow A) corresponding to the waveguide mode $m = 0$ and the additional ones (arrow B) corresponding to the mode $m = 1$.

more frequently observed as the normalized radius increases. An additional effect happens around $t/a = 0.5$ and $a/\lambda = 0.85$ ($r/a = 0.4$) (see Fig. 3). The guided-mode resonance from the fundamental and the first-order waveguide mode begin to overlap, giving rise to a very wideband reflection (very low Q) [12]. Such an effect is useful for the design of a high bandwidth mirror. The first mentioned and opposite situation, where Q is high, is useful for the design of a narrowband filter. The quality factor can thus be engineered from this map (Fig. 4), in relation with the other structural parameters.

5. ASYMMETRY AND IMPROVEMENT

In addition to the peak width, another important parameter is the peak symmetry. In many applications a symmetric peak is preferred for efficiency and it has identical sideband properties. For example, an ideal telecom filter transfer function would be a rectangular window. Here we define the asymmetry as

$$A = \frac{\nu_m - \nu_{\text{mean}}}{\Delta\nu/2}, \tag{8}$$

with ν_m as the frequency of the maximum of the peak (i.e., ν_r) and $\nu_{\text{mean}} = (\nu_1 + \nu_2)/2$. With this definition, the maximum asymmetry is $|A| = 1$, and a symmetric peak has $A = 0$. We extract the asymmetry value from the data of reflection spectra (Fig. 3) in the same way we extracted the quality factor, and we represent it in the same way also in Fig. 5, with the same remarks. We can notice regions of high and low asymmetry. To interpret the results, we represented additional information, namely, particular normalized thicknesses of the membrane. At thicknesses $t = k\lambda/(2n_2)$, $k \in \mathbf{N}$, the membrane has minimal reflection ($R = 0$) and at thicknesses $t = (2k+1)\lambda/(4n_2)$, it has maximal reflection. Therefore, we represented the positions $t/\lambda = 1/(4n_2)$, $1/(2n_2)$, $3/(4n_2)$, and $1/n_2$ in Figs. 5(a) and 5(c) (vertical dotted lines). But as the normalized radius of the holes increases, the membrane has its refractive index decreasing, in average, as we will see in Section 6. So we used the membrane effective index $n_{\text{eff-}v}$ of Eq. (13) found in Section 6 (effective index here is used in the sense "thin-film" "vertical" effective index and not "waveguide" effective index), and plotted the more representative curves of position $t/\lambda = 1/(4n_{\text{eff-}v})$, $1/(2n_{\text{eff-}v})$, $3/(4n_{\text{eff-}v})$, and $1/n_{\text{eff-}v}$ (black and white solid curves). Figure 1 gives the relation between r/a and the position $(t/\lambda, a/\lambda)$. We can see that the white curves $(t/\lambda = k/(2n_{\text{eff-}v}))$ follow regions of low asymmetry, and in particular in regions where the normalized radius is smaller, which is when the effective index approximation is the most valid. The usual top and bottom peaks of a Fano shape and related asymmetry is no more possible when the background reflectivity $R = 0$, which explains why the peaks become symmetric at thicknesses multiple of half-wavelength. The asymmetry of the peak can thus be engineered from this map (Fig. 5) in relation with the other structural parameters.

A way to get symmetric peaks for all the situations would be to apply antireflection coating [22]. In this case, the reflection will be zero around the reflection peak, which will become symmetric. In addition, a large rejection sideband will be obtained, too. For this, an antireflection layer can be added on top and below the membrane of index n_2, which was initially surrounded by a medium of index n_1 (Fig. 6 inset). The antireflection layer index is $n_3 = \sqrt{n_1 n_2}$, and its thickness is $t_3 = \lambda/(4n_3)$. In Fig. 6, we show an example of such a configuration, where the guided-mode resonance reflection peak is symmetric (peak at 533 nm, antireflection designed for 550 nm), and low reflection ($R < 2\%$) is obtained over quite a wide range ([462–861 nm] or 60% bandwidth). Note that, below 462 nm ($a/\lambda > 1$), diffraction occurs in the surrounding medium. For design purposes, the antireflection coating parameters should be matched with the guided-mode resonance position, the two being interdependent. The solution we propose here for the design is the following. Similarly to Section 3, we will use 3D FDTD to calculate the reflection spectrum, which will provide the normalized frequency a/λ of the guided-mode resonances. The input parameters are t/a,

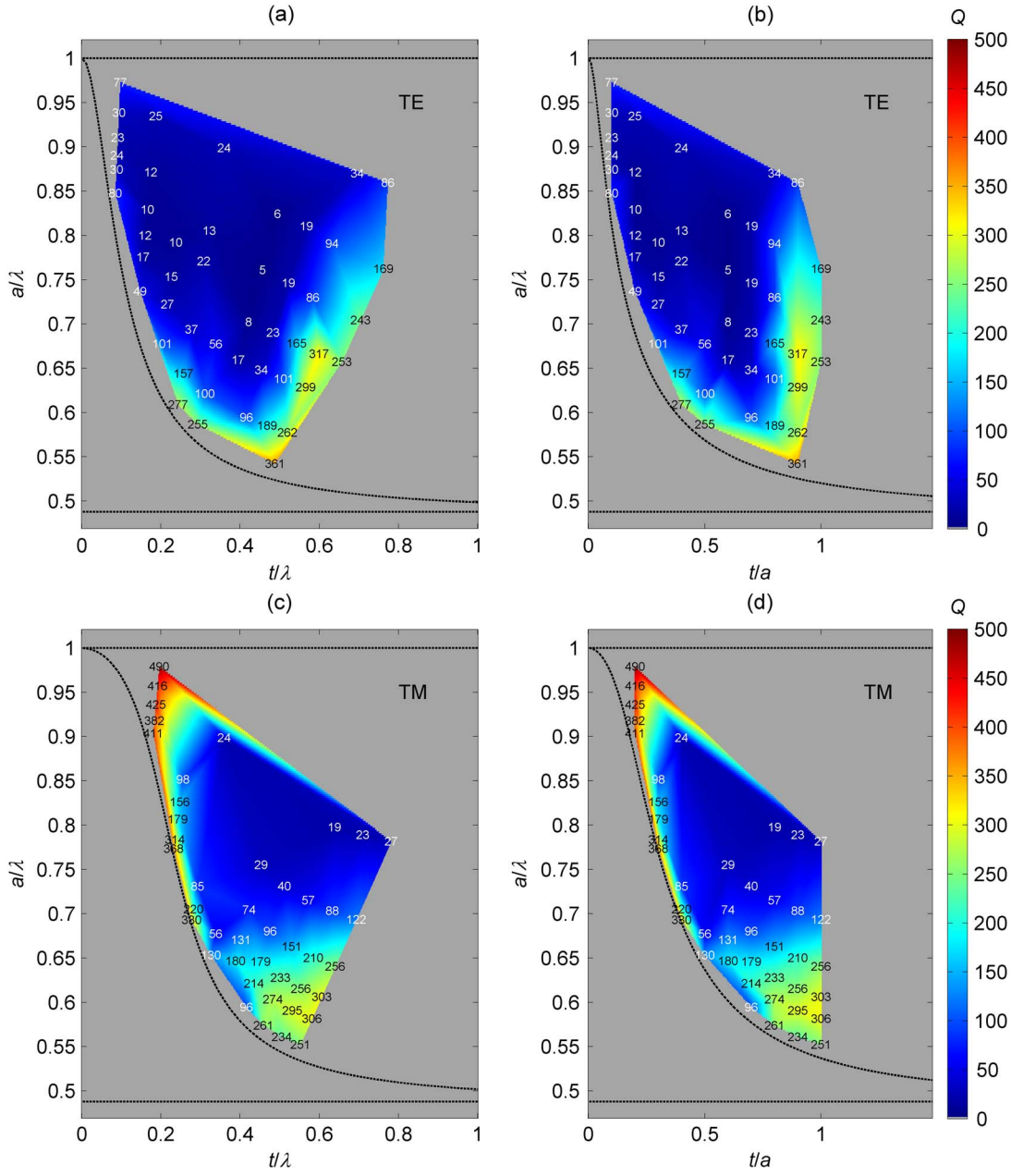

Fig. 4. (Color online) Quality factor (superimposed number and color scale) of the PhC membrane reflection peaks versus a/λ and (a) t/λ or (b) t/a, for several normalized radii r/a (see the correspondence with Fig. 1), for TE internal polarization. (c) and (d) are the same, respectively, for TM internal polarization. The theoretical limits as in Fig. 1 are also represented (dotted curves).

r/a, and t_3/a. The values t/a and r/a will be scanned as in Section 3 to produce similar color maps as in Fig. 3. For each entry of t/a and r/a, t_3/a needs to be determined. It can be decomposed as

$$t_3/a = (t_3/\lambda)/(a/\lambda) = [1/(4n_3)]/(a/\lambda), \tag{9}$$

which is indeed undetermined since a/λ is not known yet. An initial value of t_3/a can be chosen. Then from the results of the FDTD simulation, the a/λ value obtained will be reinjected into Eq. (9), and the simulation rerun. Through an iterative process, the final value of a/λ will be reached by convergence. This is only true when the normalized radius r/a tends to zero since holes will modify the "vertical" effective index of the membrane. Consequently, the antireflection layer should be adjusted accordingly. The effective index could not be extracted form the Fabry–Perot oscillations of the reflection curve (see Section 6) since they were suppressed. Nevertheless, an approximate expression developed from the case of no antireflection coating (see Section 6) can be used. However, since the antireflection is spectrally quite broad, the above-mentioned adjustment of the antireflection layer is not expected to be significant.

6. EFFECTIVE INDEX

Because of the coupling of waves propagating through the membrane and waves guided inside, and as seen in the PhC membrane reflection spectrum of Fig. 7, the PhC membrane behaves as a thin-film membrane, giving rise to Fabry–Perot

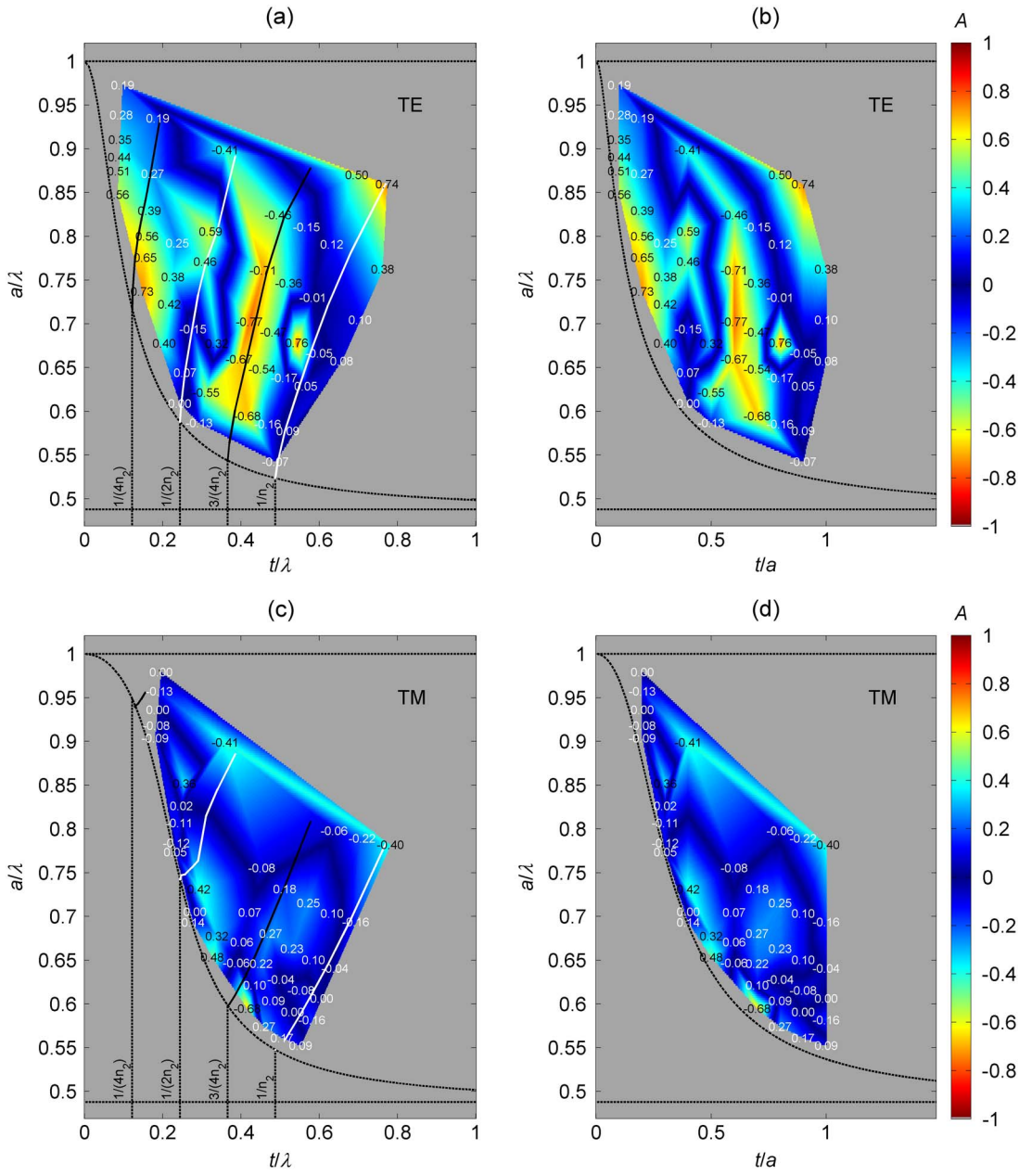

Fig. 5. (Color online) Asymmetry (superimposed number and color scale) of the PhC membrane reflection peaks versus a/λ and (a) t/λ or (b) t/a, for several normalized radii r/a (see the correspondence with Fig. 1), for TE internal polarization. (c) and (d) are the same, respectively, for TM internal polarization. The theoretical limits as in Fig. 1 are also represented (dotted curves). The black and white solid curves correspond (from left to right) to the characteristic thicknesses $t/\lambda = 1/(4n_{\text{eff-}v})$, $1/(2n_{\text{eff-}v})$, $3/(4n_{\text{eff-}v})$, and $1/n_{\text{eff-}v}$ (described in the main text).

oscillations, over which the Fano-shaped peaks of the guided-mode resonances superimpose. But the very fact of having holes in the membrane to give rise to the effect modifies its optical properties. The system then behaves, as to the background Fabry–Perot oscillations, as a membrane of effective index $n_{\text{eff-}v}$, which will depend of n_2, n_1, λ, and the geometry. The term "effective index" here is used in the sense "thin-film" "vertical" effective index and not "waveguide" effective index. From the reflection spectra obtained in Fig. 3, we extract this effective index. To this purpose, we calculate the reflection of a Fabry–Perot cavity composed of a membrane of index n_m and thickness t, surrounded by a medium of index n_1, according to

$$R_{\text{FP}} = 1 - \frac{(1-R_i)^2}{1+R_i^2 - 2R_i\cos\left(\frac{2\pi}{\lambda}2n_m t\right)}, \tag{10}$$

with

$$R_i = \left(\frac{n_1 - n_m}{n_1 + n_m}\right)^2. \tag{11}$$

We scan the value of n_m, and find manually the best matching in position and amplitude of the Fabry–Perot oscillations compared to the background of the reflection of the PhC membrane, around the position of the first guided-mode

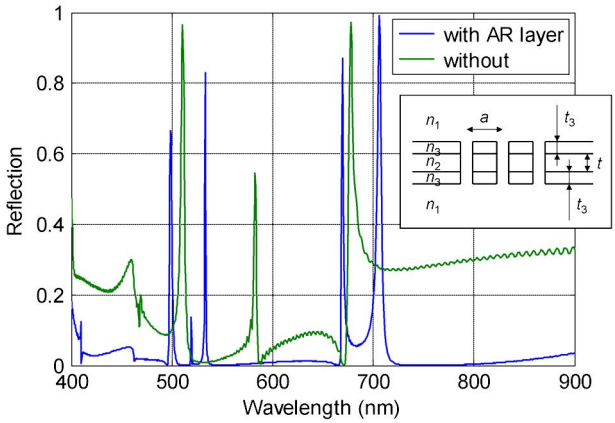

Fig. 6. (Color online) Reflection spectrum of a PhC membrane ($r/a = 0.2$, $t = 134\,\text{nm}$, $a = 462\,\text{nm}$), without (green curve) and with (blue curve) an antireflection (AR) layer above and below it designed for $\lambda = 550\,\text{nm}$. Inset: schematic of the PhC membrane with antireflection layers.

resonance (see an illustration in Fig. 7), which gives $n_{\text{eff-}v}$. For a given normalized radius r/a, the values we found for the different normalized thicknesses t/a are close, generally at ± 0.01 from the average, for both TE and TM internal polarization. For the highest r/a values, no effective index could be extracted from small t/a values because the background Fabry–Perot oscillations can no more be discerned: indeed, their amplitude decreases, their spacing in frequency increases, and the guided-mode resonance peaks are wider. The values of effective index are reported in Fig. 8 versus the size of the holes.

We now try to compare it with theoretical models. We represented in Fig. 8 for comparison the effective index obtained by averaging the refractive index, with respect to the fraction $f = \pi(r/a)^2$ occupied by the medium of index n_1 and that of the medium of index n_2, i.e., according to

$$n_{\text{eff-}v1} = f n_1 + (1-f) n_2. \tag{12}$$

This arithmetic mean gives a straight line on the graph. We also represented the quadratic mean that corresponds to the arithmetic mean of the dielectric constant $\varepsilon = n^2$:

$$n_{\text{eff-}v2} = (f n_1^2 + (1-f) n_2^2)^{\frac{1}{2}}, \tag{13}$$

and the averaging corresponding to the harmonic mean of ε:

$$n_{\text{eff-}v3} = (f n_1^{-2} + (1-f) n_2^{-2})^{-\frac{1}{2}}. \tag{14}$$

These last two expressions are exact effective indices for particular cases, such as one-dimensional periodic structures, for propagation along the periodic plates and polarization, respectively, parallel and perpendicular to the plates [23]. But

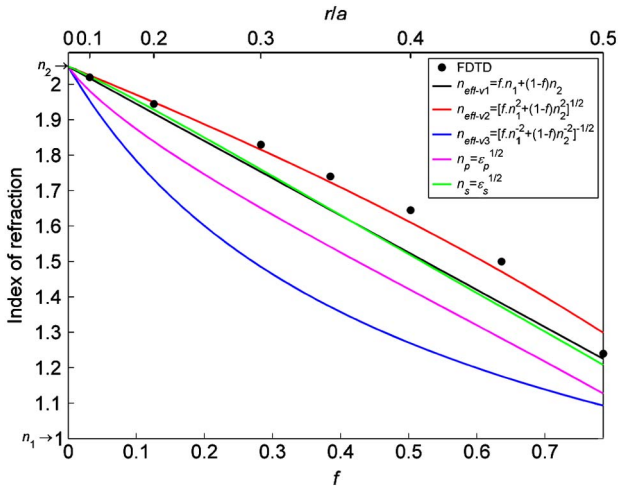

Fig. 8. (Color online) Effective index $n_{\text{eff-}v}$ of the PhC membrane versus area filling factor (f) of the holes and their normalized radius r/a. Dots represent the value extracted from FDTD simulations, and colored curves correspond to different theoretical models.

no closed-form expression is available for light propagating along rods or holes of a 2D structure. Nevertheless, lower and upper bounds of the dielectric constant can be determined [24]. For our case of a square lattice of cylinders, these are, respectively,

$$\varepsilon_p = \varepsilon_2 \cdot \left(1 - 2\frac{r}{a} + \frac{2}{\frac{1}{L} - 1} \cdot \left[\frac{\pi}{4} - \frac{\arctan\left[\left(\frac{1-G}{1+G} \right)^{\frac{1}{2}} \right]}{(1-G^2)^{\frac{1}{2}}} \right] \right), \tag{15}$$

$$\varepsilon_s = \varepsilon_2 \cdot \left(1 - 2\frac{r}{a} + \frac{\pi}{2(L-1)} - \frac{\ln\left[\frac{H+1+(H^2-1)^{\frac{1}{2}}}{H+1-(H^2-1)^{\frac{1}{2}}} \right]}{(L-1)(H^2-1)^{\frac{1}{2}}} \right)^{-1}, \tag{16}$$

with $G = 2\frac{r}{a}(\frac{1}{L} - 1)$, $H = 2\frac{r}{a}(L-1)$, $L = \frac{\varepsilon_1}{\varepsilon_2}$, $\varepsilon_1 = n_1^2$, $\varepsilon_2 = n_2^2$, and for $\frac{r}{a} \le \frac{1}{2}$. We added these values in Fig. 8 and notice that the ones extracted from FDTD are not contained within. But all the effective index approximations are valid only when the period is much smaller than the wavelength, which explains why we deviate from the theory, as our periods are not very small compared to the wavelengths. Interestingly, Eq. (13) eventually gives empirically an approximation of the effective index. It can be conveniently used for a reconstruction of the reflection spectrum of the PhC membrane [background part, Eq. (10)]. The error is $<1\%$ for values of $r/a \le 0.35$.

We just discussed the "vertical" effective index, which matters for the background reflection. Let us now discuss the "horizontal" effective index (still different from the "waveguide" effective index), which will matter for the guided-mode

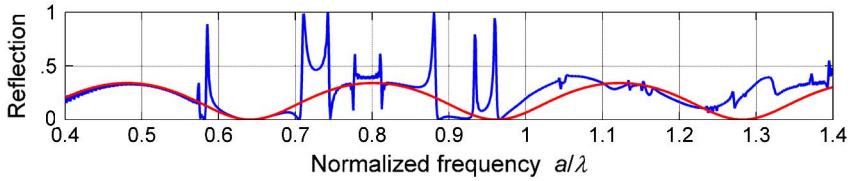

Fig. 7. (Color online) Reflection spectrum of a PhC membrane ($r/a = 0.2$, $t/a = 0.8$) (blue curve, with peaks) and reflection spectrum of a Fabry–Perot membrane of index $n_m = 1.95$ (red curve, slowly varying), which has been matched to the former.

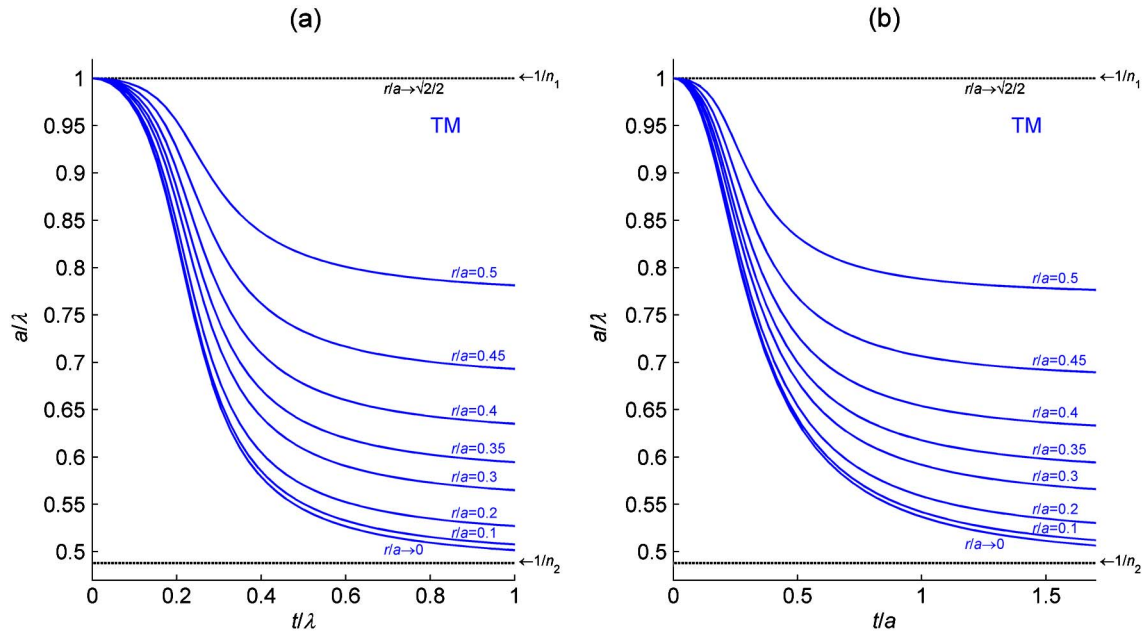

Fig. 9. (Color online) Positions of guided-mode resonances in normalized frequency a/λ versus the normalized thickness of the PhC membrane (a) t/λ or (b) t/a for varying hole normalized radius r/a for TM internal polarization, obtained using the "horizontal" effective index in the model of infinitely small holes.

resonance positions. For the propagation in the plane perpendicular to the rods or holes of a 2D structure, a closed-form expression is available for the effective index [25], but only for polarization along the rods or holes, i.e., TM internal polarization for our case. This expression is the same as in Eq. (13):

$$n_{\text{eff-}h} = (f n_a^2 + (1-f) n_b^2)^{\frac{1}{2}}, \tag{17}$$

for media of index n_a and n_b. For the in-plane propagation, our PhC membrane structure can be seen as a 2D structure, with a material of index n_{eff} (the planar waveguide effective index) perforated by holes of index n_1. The "horizontal" effective index of the PhC membrane is then

$$n_{\text{eff-}h} = (f n_1^2 + (1-f) n_{\text{eff}}^2)^{\frac{1}{2}}. \tag{18}$$

In order to predict the positions of the guided-mode resonance for varying radius in a simplified way, we reused the calculations for infinitely small holes, but now applying the "horizontal" effective index. That is to say, the guided-mode resonance positions are now given by

$$\frac{a}{\lambda_1} = \frac{1}{n_{\text{eff-}h}}, \tag{19}$$

instead of Eq. (1), and they are calculated using Eqs. (18) and (2). The results for TM polarization are plotted in Fig. 9. They agree quite well with the FDTD simulations (Fig. 1) when the normalized radius r/a is not too large. The error is $<2\%$ for values of $r/a \le 0.35$, and is $<1\%$ for values of $r/a \le 0.3$ and $t/a \le 0.7$. Even though the periods are not very small compared to the wavelengths, this effective index approximation gives good results and can be used for a reconstruction of the reflection spectrum of the PhC membrane [guided-mode resonance positions part, Eq. (19)].

Finally, using the Fabry–Perot background [Eq. (10) with Eq. (13)], the guided-mode resonance positions [Eq. (19) with Eqs. (18) and (2)], and the shape of the Fano peaks [16], the reflection spectrum of the PhC membrane around the first guided-mode resonance in TM internal polarization could be completely reconstructed, with a limited error for this simplified model.

7. CONCLUSION

We have presented a study of guided-mode resonances present in PhC slabs. Their position can be designed using the figures produced here, along with the peak characteristics (quality factor and asymmetry), and we gave a global view of their behavior. Further improvement of peak symmetry with rejection sidebands using antireflection coating has been shown for these 2D PhC membranes. Finally, we discussed the effective index corresponding to these structures and showed that the reflection spectrum can be reconstructed with a good precision using a simplified model.

ACKNOWLEDGMENTS

This work was supported by the Natural Sciences and Engineering Research Council of Canada (NSERC), Strategic Grant 336830-2006.

REFERENCES

1. R. W. Wood, "On a remarkable case of uneven distribution of light in a diffraction grating spectrum," Proc. Phys. Soc. London **18**, 269–275 (1902).
2. A. Hessel and A. A. Oliner, "A new theory of Wood's anomalies on optical gratings," Appl. Opt. **4**, 1275–1297 (1965).
3. M. Nevière, "The homogeneous problem," in *Electromagnetic Theory of Gratings*, R. Petit, ed. (Springer-Verlag, 1980), pp. 123–157.
4. K. B. Crozier, V. Lousse, O. Kilic, S. Kim, S. Fan, and O. Solgaard, "Air-bridged photonic crystal slabs at visible and near-infrared wavelengths," Phys. Rev. B **73**, 115126 (2006).

5. R. Magnusson and S. S. Wang, "New principle for optical filters," Appl. Phys. Lett. **61**, 1022–1024 (1992).
6. S. Tibuleac and R. Magnusson, "Reflection and transmission guided-mode resonance filters," J. Opt. Soc. Am. A **14**, 1617–1626 (1997).
7. C. F. R. Mateus, M. C. Y. Huang, L. Chen, C. J. Chang-Hasnain, and Y. Suzuki, "Broad-band mirror (1.12–1.62 μm) using a subwavelength grating," IEEE Photon. Technol. Lett. **16**, 1676–1678 (2004).
8. V. N. Astratov, R. M. Stevenson, I. Culshaw, D. M. Whittaker, M. S. Skolnick, T. F. Krauss, and R. M. De La Rue, "Heavy photon dispersions in photonic crystal waveguides," Appl. Phys. Lett. **77**, 178–180 (2000).
9. W. Suh and S. Fan, "All-pass transmission or flattop reflection filters using a single photonic crystal slab," Appl. Phys. Lett. **84**, 4905–4907 (2004).
10. C. Kappel, A. Selle, M. A. Bader, and G. Marowsky, "Double grating waveguide structures: 350-fold enhancement of two-photon fluorescence applying ultrashort pulses," Sens. Actuators B **107**, 135–139 (2005).
11. N. Ganesh, W. Zhang, P. C. Mathias, E. Chow, J. A. N. T. Soares, V. Malyarchuk, A. D. Smith, and B. T. Cunningham, "Enhanced fluorescence emission from quantum dots on a photonic crystal surface," Nat. Nanotechnol. **2**, 515–520 (2007).
12. L. Shi, P. Pottier, M. Skorobogatiy, and Y.-A. Peter, "Tunable structures comprising two photonic crystal slabs—optical study in view of multi-analyte enhanced detection," Opt. Express **17**, 10623–10632 (2009).
13. S. Boutami, B. Ben Bakir, J.-L. Leclercq, X. Letartre, C. Seassal, P. Rojo-Romeo, P. Regreny, M. Garrigues, and P. Viktorovitch, "Photonic crystal-based MOEMS devices," IEEE J. Sel. Top. Quantum Electron. **13**, 244–252 (2007).
14. Y. Kanamori, T. Kitani, and K. Hane, "Control of guided resonance in a photonic crystal slab using microelectromechanical actuators," Appl. Phys. Lett. **90**, 031911 (2007).
15. W. Suh, M. F. Yanik, O. Solgaard, and S. Fan, "Displacement-sensitive photonic crystal structures based on guided resonance in photonic crystal slabs," Appl. Phys. Lett. **82**, 1999–2001 (2003).
16. S. Fan, W. Suh, and J. D. Joannopoulos, "Temporal coupled-mode theory for the Fano resonance in optical resonators," J. Opt. Soc. Am. A **20**, 569–572 (2003).
17. S. Peng and G. M. Morris, "Experimental demonstration of resonant anomalies in diffraction from two-dimensional gratings," Opt. Lett. **21**, 549–551 (1996).
18. M. S. Sodha and A. K. Ghatak, *Inhomogeneous Optical Waveguides* (Plenum, 1977), pp. 5–29.
19. B. E. A. Saleh and M. C. Teich, *Fundamentals of Photonics* (Wiley, 1991), pp. 238–271.
20. S. G. Johnson, "Meep," http://ab-initio.mit.edu/wiki/index.php/Meep.
21. S. G. Johnson, "Meep Tutorial/Band diagram, resonant modes, and transmission in a holey waveguide," http://ab-initio.mit.edu/wiki/index.php/Meep_Tutorial/Band_diagram%2C_resonant_modes%2C_and_transmission_in_a_holey_waveguide.
22. S. S. Wang and R. Magnusson, "Design of waveguide-grating filters with symmetrical line shapes and low sidebands," Opt. Lett. **19**, 919–921 (1994).
23. M. Born and E. Wolf, *Principles of Optics*, 7th ed. (Cambridge University, 1999), pp. 790–852.
24. S. R. Coriell and J. L. Jackson, "Bounds on transport coefficients of two-phase materials," J. Appl. Phys. **39**, 4733–4736 (1968).
25. P. Lalanne and M. Hutley, "Artificial media optical properties—subwavelength scale," in *Encyclopedia of Optical Engineering*, R. Driggers, ed. (Marcel Dekker, 2003), Vol. 1, pp. 62–71.